geosciences

Article

Hydrological Characteristics of Columnar Basalt Aquifers: Measuring and Modeling Skaftafellsheiði, Iceland

Roel Dijksma [1],*, Victor Bense [1], Eline Zweers [1], Lisette Avis [2] and Martine van der Ploeg [1]

[1] Hydrology and Environmental Hydraulics Group, Wageningen University,
6708 PB Wageningen, The Netherlands; victor.bense@wur.nl (V.B.); eline.zweers@wur.nl (E.Z.);
martine.vanderploeg@wur.nl (M.v.d.P.)
[2] Royal Haskoning DHV, 3818 EX Amersfoort, The Netherlands; lisette.avis@rhdhv.com
* Correspondence: roel.dijksma@wur.nl

Abstract: Basalt with columnar jointing can act as a good groundwater conductor. In areas with limited water resources in sedimentary rock, such as the Deccan Traps in India and the Columbia River basalt formations in Washington State (USA), large quantities of groundwater are abstracted from such basalt formations for drinking water supply and irrigation. The hydraulic properties of basaltic formations are difficult to quantify. To obtain a better understanding of their hydraulic properties, intensive field campaigns in Iceland were combined with a conceptual groundwater model in MODFLOW. The field experiments enabled us to derive the upper boundary conditions, like precipitation surplus, and obtain reliable ranges for the k_h (0.01–0.3 m d^{-1}) and k_v (0.01–10 m d^{-1}) of the basalt formations. The main objective was to test the concept of representative elementary volumes (REVs) for such basaltic regions. Precipitation excess for the Vestragil and Eystragil catchments was calculated by taking into account the orographic effect of precipitation. It was found that at higher elevations (600 m + msl) the precipitation was twice the amount compared to the base camp rain gauge at 100 m + msl. Calculated evapotranspiration (1–2 mm d^{-1}) is in line with the literature. In the MODFLOW model, best results were obtained when the top layer (organic soil, peat, and regolith) was considered to be most conductive (up to 10 m d^{-1}), with a gradual reduction in hydraulic conductivity with depth in the basaltic aquifers. This study shows that, when larger elementary volumes are used, a good model representation of basaltic regions can be created.

Keywords: basalt; field study; MODFLOW; representative elementary volume; groundwater flow

1. Introduction

Basalt, a mafic extrusive igneous rock type, is the most dominant rock type of ocean crust, but it can also cover large areas on continents. Often, these so-called flood basaltic regions are the result of flood basalt eruptions related to the development of mantle plumes. Depending on the composition of the lava and the cooling processes, columnar polygons can develop. The voids, fissures, and fractures between the columnar polygons are conductive to groundwater. Additionally, the interfaces between subsequent flows can be a groundwater conduit. Areas with extensive and thick basaltic aquifers are often used for drinking water production and irrigation purposes, with numerous drilled or dug wells. Examples of such regions are the Columbia River Basalt Group in northwest USA [1] and the Deccan Traps [2] in India. The Columbia Plateau basaltic rock aquifers cover an area of more than 100,000 km^2 [1,3], with the Deccan basalts even reaching 500,000 km^2.

The Deccan basalts have a succession of more than 2 km of flat-lying basalt lava flows [2]. Over the past decades, groundwater levels in such basaltic aquifers have been declining dramatically [4,5]. This decline is often caused by both increased water use and reduced recharge as a result of climate change impacts on the water cycle, but is also related to the limited effective porosity and storage of basalt formations [1].

Moreover, the relation among rainfall, storage capacity, and runoff in such basaltic regions is often poorly understood, with over-abstraction as a result [5–9]. The uncertainty in the physical properties is related to the size and shape of the cooling joints (hexagonal formations).

Domenico and Schwartz [10] showed that the effective physical parameters like porosity and hydraulic conductivity are highly dependent on the sampled volume (Figure 1). Only when the sample includes multiple lava flows can representative values be obtained, i.e., the representative elementary volume (REV).
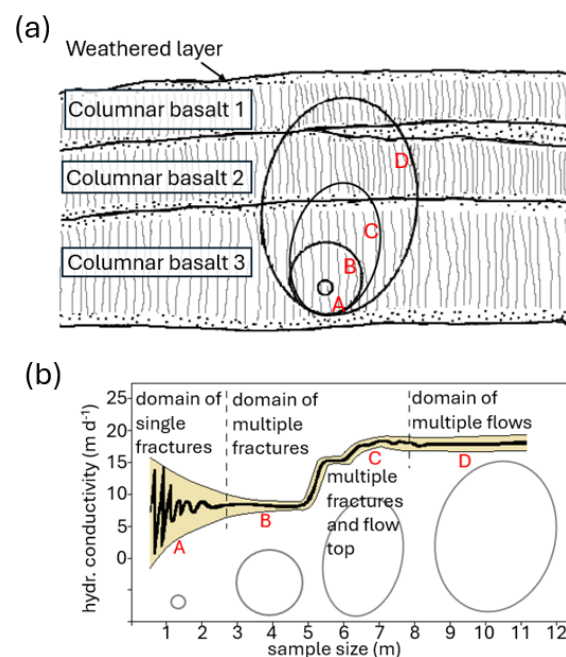

Figure 1. Representative Elementary Volume in basalt, with (**a**) sampling volumes in an imaginary three-layer columnar basalt area, and (**b**) the relation between sample volume and hydraulic conductivity modified from [2].

In order to calculate scenarios for sustainable future water use from these basaltic aquifers, groundwater models with good estimates for the physical parameters are needed. A major problem in groundwater modeling in basaltic areas is the limited accessibility to the basalt aquifers for measuring their physical properties. Our aim is to obtain a better understanding of these properties and their impacts on the basaltic aquifers to aid subsequent modeling in the area of Skaftafellsheiði, southeast Iceland. Skaftafellsheiði is a small basaltic catchment (4 × 6 km), with elevation levels ranging from 100 m + msl in the south to 1000 m + msl in the north (see Figure 2) [11,12].
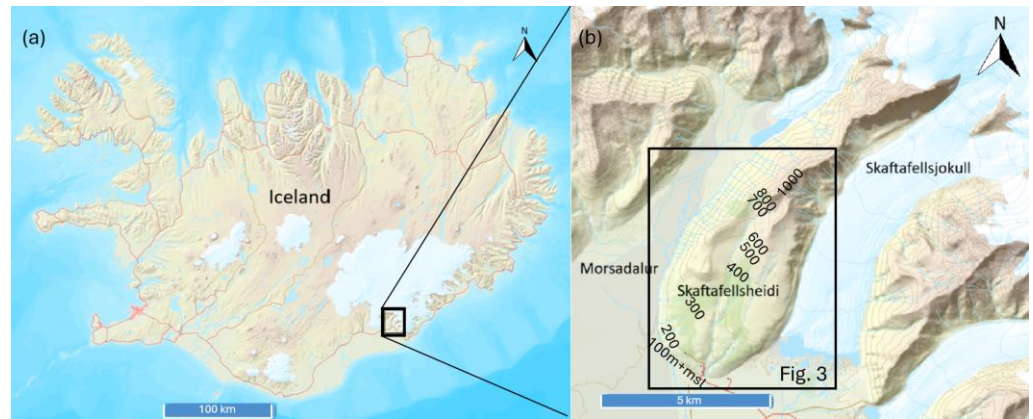
Figure 2. (**a**) Topography of Iceland, and (**b**) Skaftafellsheiði in southeast Iceland. Adapted from [13].

The basalt layers in the study area originate from a periglacial period in the Late Tertiary (4–5 MA B.P.). The lava flows are interbedded with some weathered and/or sedimentary interbeds, which might have undergone contact metamorphism [14–16]. The basalt formations dip toward the south at an angle of approximately 10 to 15 degrees. During the Pleistocene glaciations, glacier tongues created the deep valleys to the east and west of Skaftafellsheiði (Skaftafellsdalur and Morsadalur, respectively). The northeast section of Skaftafellsheiði has a sharp mountain ridge which has not been glaciated. The southern part of Skaftafellsheiði has been glaciated. Because of these glaciations, the younger layers have been eroded, and a rather smooth dome shape with exposed older Tertiary basalt formations remains. The result of all these eruptions and glacial weathering is an isolated > 1000 m high basaltic ridge with multiple basalt flows. Figure 3 shows a detailed geological map of the southern part of Skaftafellsheiði, adapted from [17].
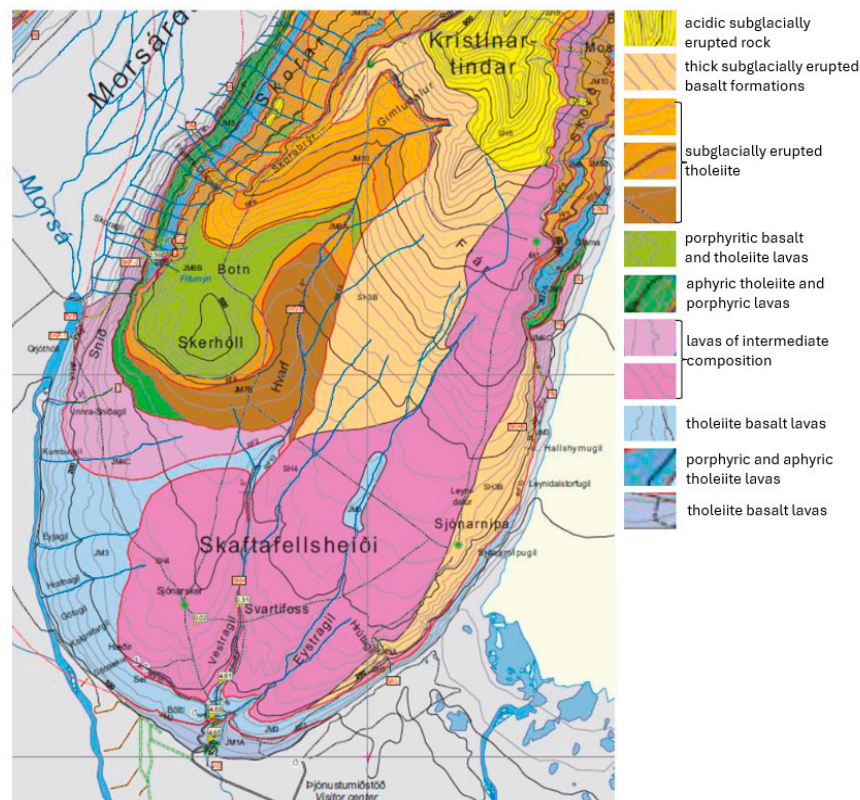
Figure 3. Geological map of Skaftafellsheiði and surroundings, adapted from [17].

At the highest elevations in the catchment area, acidic subglacially erupted rock can be found (yellow in Figure 3). This formation consists of columnar basalts. Further south, this formation has been eroded during glaciations. This implies that, at lower elevations, older basaltic formations are outcropping. Svartifoss waterfall in Vestragil (see Figure 3) was used to obtain detailed information on the deeper, thus older, basalts. The oldest flows are found at the foot of the basalt dome, where the Eystragil and Vestragil are discharging into the Skeiðararsandur. During the field campaign, dikes were also found. These dikes develop when the lava is forcing through older basalt formations. All the formations indicated in Figure 3 show columnar hexagonal structures and can, therefore, be considered to be aquifers or aquitards, depending on the void aperture. The dikes in the area are very poor water conductors and act as water barriers. This leads to a hydrogeological description of Skaftafellsheiði as being a multiple aquifer system with a hydraulic conductivity decreasing with depth, with some hydraulic compartmentations due to dike intrusions.

Skaftafellsheiði has two main streams that cut into the upper basalt layers during the Holocene, i.e., the Eystragil and Vestragil (see Figure 3). The basalt formations are covered by some weathered basalts (regolith layer) and/or organic layers (peat). This explains the morphology of the basalt formations, with a sharp ridge in the northerly section, the rounded top further south, the steep slopes toward the glacier valleys, and the V-shaped stream incisions. From the southern tip of Skaftafellsheiði, water flows onto the Skeiðararsandur, consisting of a 100 m thick gravel and coarse sand layer. This Skeiðararsandur runs approximately 26 km south, ending up in the Atlantic Ocean. This rather isolated, well-defined area with basalt formations and a characteristic water flow can serve as a suitable study area.

Because of the weathering processes that occurred during the glaciations, physical properties like the thickness of the subsequent flows of the deeper basalt flows can be studied on the dome flanks.

Hydrogeology

The porosity and hydraulic conductivity (k) of the basalt formations are expected to decrease from the relatively younger upper basalt layers to the deeper basalt layers. This is because it is expected that the fractures between the basaltic polygons decrease in width with depth [18]. The pressure on the formations and, therefore, the fractures is higher, causing the fractures to open less easily [19,20]. The so-called scrambled-egg layer between subsequent flows—consisting of weathered basalt and paleosols—can act as an aquifer and, depending on contact metamorphism, also as an aquitard.

During the Holocene, a relatively thin peat layer (<1 m) developed. This peat layer acts as a thin aquifer and water storage because of its high storage coefficient.

On the flanks of Skaftafellsheiði, numerous small streams can be observed (see also Figure 3). These streams appear to be draining predominantly the peat and the upper basalt formation. This was acknowledged during the field campaigns, where hardly any water seemed to come from springs in the deeper basalt layers. Therefore, we can safely assume that the topographical boundary coincides with the hydrological boundary.

Vegetation

Land cover at Skaftafellsheiði predominantly consists of low vegetation, with some small trees near the catchment outlet. Most vegetation belongs to the categories of peat, moss, and shrubs. The leaf area index (LAI) for these types of vegetation is low. The vegetation cover was described in detail in the 1980s [12] and confirmed during the field campaigns in 2016 and 2023. At the lower ranges (100–200 m + msl), a low deciduous forest was found (*Betula*, *Salix*, *Sorbus*), followed, in the range of 200–300 m + msl, by peaty soil covered with dwarf shrubs (*Betula*, *Salix*, *Juniperus*) and mosses. Figure 4 shows the vegetation zones [21].
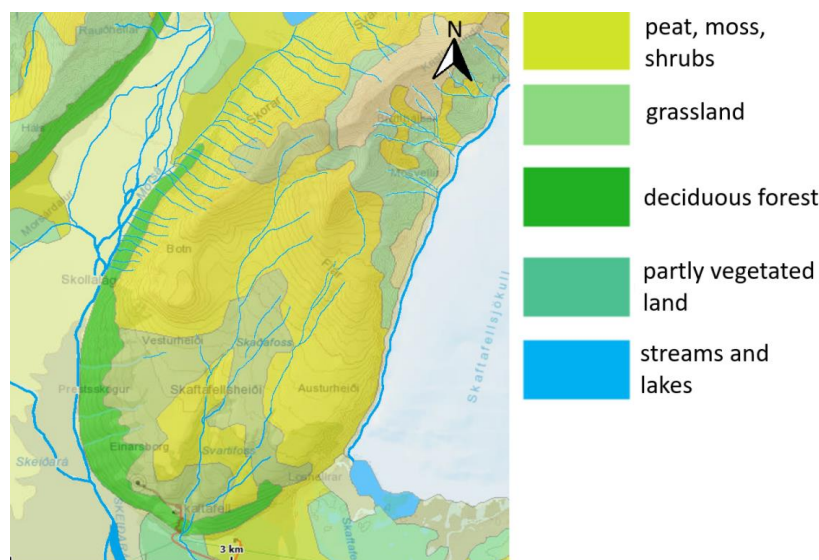
Figure 4. Vegetation zones in the south part of Skaftafellsheiði [21], indicating the deciduous forest (predominantly *Betula*, *Salix*, and *Sorbus*) at lower elevations, partly vegetated peat soils covered with dwarf shrubs in the range of 200–300 m + msl, and peat moss and small shrubs at higher elevations.

Climate

According to the Köppen–Geiger classification [22], Iceland is classified as polar tundra (ET). However, the warm Gulf Stream that touches the south coast of Iceland brings a warm temperate climate (Cfb) along the coastline. Rainfall in Iceland is evenly spread year-round, but does have a pronounced orographic effect and, thus, large spatial variation. On upwind sides of topographical obstructions like volcanoes and glaciers, the rain can annually reach >4000 mm y^{-1}, while on downwind regions, it amounts to <400 mm y^{-1}. The study area on Skaftafellsheiði is within the warm temperate climate (Cfb) zone, with an average annual precipitation of approximately 1600 mm. Table 1 provides long-year averaged (1961–1990) temperature and precipitation data from the meteorological station Kirkjubæjarklaustur, about 60 km southwest of Skaftafellsheiði.

Table 1. Long year averaged precipitation (P in mm) and temperature (T in °C) at Kirkjubæjarklaustur [23].

	January	February	March	April	May	June	July	August	September	October	November	December	Avg
P	145	130	130	115	118	131	121	159	141	185	137	133	137
T	−0.4	0.2	0.7	3.2	6.5	9.4	11.2	10.4	7.5	4.5	1.1	−0.4	4.5

2. Materials and Methods

2.1. Field Campaign Setup

The field campaigns were conducted to (1) obtain a good, detailed overview of the subsequent basalt formations, (2) gather information on the various hydrological components of the water balance, and (3) collect spatially distributed hydrological data as the upper boundary for a groundwater flow model.

Water Balance

For practical reasons, the water balance approach was selected for use in combination with the acquired field data and information. This approach was used for the combined catchments of Eystragil and Vestragil, according to Equation (1).
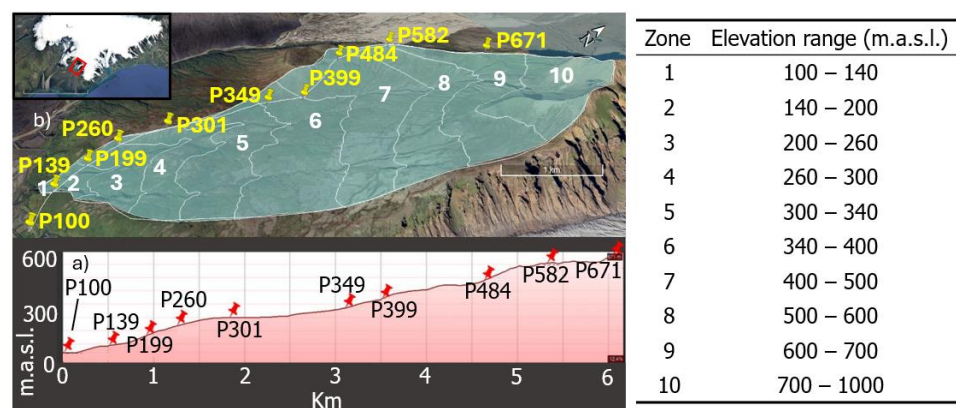
$$\Delta S = P + M - Q - ET \tag{1}$$

where ΔS is the storage change, P is the precipitation, M is the snowmelt water, Q is the discharge of Eystragil and Vestragil, and ET is the evapotranspiration, all in m^3 for the duration of the field campaigns.

Data for all components of the water balance were collected during field campaigns for the periods 12 July–6 September 2015 and 9 May–11 June 2023. These field campaigns were short compared to the usual duration of water balance studies (56 and 33 days, respectively). However, because of the temporal distribution of the rainfall (according to its climate zone, evenly spread year-round), in combination with the low-storage capacity and poor accessibility for most of the year, it was decided to work with these short intensive field campaigns.

Storage change (ΔS) was not measured directly during the field campaign. It was assumed that the porosity of the basalt formations would be very low, in the range of 1–5% [19]. Most of the ΔS was expected to occur in the relatively thin peat layer (<1 m) in the elevation range of 300–700 m + msl. Because of the variable topography and peat cover thickness, the range of inaccuracy in translating point measurements into a spatially distributed ΔS was expected to be large. Additionally, it was expected that the ΔS would be relatively small compared to the inaccuracy of the other water balance components, despite the rather short field campaigns. Therefore, it was decided to compute the ΔS via the water balance approach and to relate that to general field observations at the start and end of both field campaigns.

Precipitation (P) was measured by using handmade totalizers (rain gauges). In the 2015 field campaign, in total, seven rain gauges were installed to quantify the orographic effect of precipitation at Skaftafellsheiði [24]. One rain gauge was installed at the Skaftafell campsite, at the foot of Skaftafellsheiði (100 m + msl). This rain gauge was considered the home base rain gauge and was measured on a daily basis. Further uphill, gauges were installed at 300, 500, and 700 m + msl, with a gauge further east and another gauge further west at every elevation. These rain gauges were measured at three-day intervals. In 2023, in total, 10 rain gauges were installed. They were placed on the west side of the basalt dome, in a relatively straight line with elevations of 100, 140, 200, 260, 300, 350, 400, 480, 580, and 680 m + msl. For all rain gauges, P-zones were defined with an elevation range and an area. The rain gauges and linked elevation ranges are presented in Figure 5. The gauges at 100, 140, 200, 260, 300, 350, and 400 m + msl were measured on a daily basis, while the gauges at 480, 580, and 680 m + msl were measured every three days. In order to generate daily precipitation data, the higher elevation zones were calculated by computing the correlation with their closest rain gauge. Through this correlation coefficient, the cumulative 3-day precipitation was distributed over these 3 days.

Zone	Elevation range (m.a.s.l.)
1	100 − 140
2	140 − 200
3	200 − 260
4	260 − 300
5	300 − 340
6	340 − 400
7	400 − 500
8	500 − 600
9	600 − 700
10	700 − 1000

Figure 5. (**a**) Rain gauge locations on a cross-section of the study area, with red pins indicating the rain gauge and the numbers indicating the elevations in m + msl. (**b**) Precipitation zones for the 2023 field campaign at Skaftafellsheiði. The yellow pins indicate the locations of the rain gauges.

Snowmelt (*M*) was estimated by visual observations and pictures of snow coverage in the catchment in combination with measurements of snow thickness obtained during the field campaigns. Snow coverage and thickness were translated into water volumes using the snow water equivalent (SWE) (−) [25].

Discharge (*Q*) was measured at the outlet of Eystragil and Vestragil (i.e., where the streams leave the Skaftafellsheiði and enter the Skeiðararsandur) by using automatic pressure transducers with a measuring interval of 15 min. The pressure transducers recorded the water level variations in both streams. These water levels were transferred into discharges via a rating curve derived from hand measurements under various discharge conditions. It was expected that the inaccuracy of this method would be rather high. Eystragil and Vestragil were measured just downstream of the last waterfall, where the streams flow onto the Skeiðararsandur. Part of the discharge might have already been infiltrating into the sandur gravels. Based on the expectation that this infiltration would be constant, it was anticipated that base flow conditions would be more heavily influenced by this measuring inaccuracy than the peak flows.

Evapotranspiration was derived using the Hargreaves–Samani equation (see Equation (2)) [26–28]. Temperature, relative humidity, wind speed, and wind direction data were obtained from the nearest weather station, which is at Kirkjubæjarklaustur, at a 60 km distance in a southwesterly direction. The weather station lies in the same climate zone (Cfb) as the research area.

$$ET_{ref} = 0.051(1-\alpha)R_s\sqrt{T+9.5} - 2.4\left(\frac{R_S}{R_A}\right)^2 + 0.048(T+20)\left(1-\frac{R_H}{100}\right)(0.5+0.536\mu) + 0.00012Z \qquad (2)$$

Valiantzas [28] recommended a value of 0.25 for albedo (*α*). R_S is the solar radiation at the Earth surface (MJm^{-2} d^{-1}), *T* (C) is the average daily temperature, R_A is the extraterrestrial radiation (MJm^{-2} d^{-1}), R_H is the relative humidity (%), *μ* is the wind speed (m s^{-1}), and *Z* is the elevation (m + msl).

$$R_S = K_T R \propto (T_{max} - T_{min})^{0.5} \qquad (3)$$

K_T (°C$^{0.5}$) is recommended to be 0.19 for coastal regions by Hargreaves and Samani [26].

$$R_A = 3N sin(0.13N - 0.95\varphi) \qquad (4)$$

N is the number of daylight hours and *φ* is the latitude of the site in radians.

Reference evapotranspiration (ET_{ref}) is a measure for the evapotranspiration of grass-covered soils. When the vegetation cover differs from grass, a correction factor is needed, i.e., the crop factor K_c (−). A $K_c > 1$ indicates that the vegetation has a higher evapotranspiration than grass vegetation under identical meteorological conditions. Field observations also showed that the vegetation was not fully covering the surface at all elevation ranges. Therefore, a vegetation coverage factor f_c (−) was also introduced (see Equation (5)). Table 2 shows the parameters required to calculate ET$_{pot}$.

$$ET_{pot} = f_c K_c ET_{ref} \qquad (5)$$

Precipitation (*P*) and evapotranspiration (ET$_{pot}$) data were used to create rain surplus data (P_{excess}) for each elevation zone. ET_{pot} was expected to provide a good representation of the actual evapotranspiration (ET_{act}), as the catchment never faced very long dry spells with insufficient water available for the vegetation.

Table 2. Crop factors (k_c) and vegetation coverage (f_c) per elevation range [21,29].

Zone	Vegetation Type	Elevation Range (m + msl)	K_c	f_c
1	Deciduous forest	100–200	0.9	0.9
2	Peat (willows)	200–300	0.9	0.8
3	Peat (bog, forest, grass)	300–400	0.9	1
4	Moss	400–540	0.15	0.6
5	Vegetated regolith	540–700	0.45	0.45
6	Bare regolith	700–1000	0.2	0

2.2. Model Setup

The model of the study area was constructed in the 3D groundwater flow model MODFLOW [30,31]. Even though it was emphasized that information on the basalt flows and their physical properties was rather limited and, at points, almost anecdotal (based on expert judgement), the model alternatives (alternatives for a spatially distributed numerical model like MODFLOW) were expected to have even larger uncertainties, which would reduce the usefulness of the model [32]. The MODFLOW model boundary was topography-based [21,33]. For all boundaries, no-flow Neumann boundary conditions were applied. The base of the model was set to 90 m + msl, which is 10 m lower than the Eystragil and Vestragil outlet level (100 m + msl). The grid consisted of cells of 50 × 50 m and there were 10 model layers (see Figure 6). Table 2 summarizes the model setup and the hydrogeological properties of the materials. The basalt was divided into seven model layers. These do not resemble actual basalt flows, yet enabled us to decrease the hydraulic conductivity as a function of depth [11,34]. From the concept of the representative elementary volumes (REVs) [10], it was assumed that it would not be necessary to exactly mimic the real basalt formations in the model.
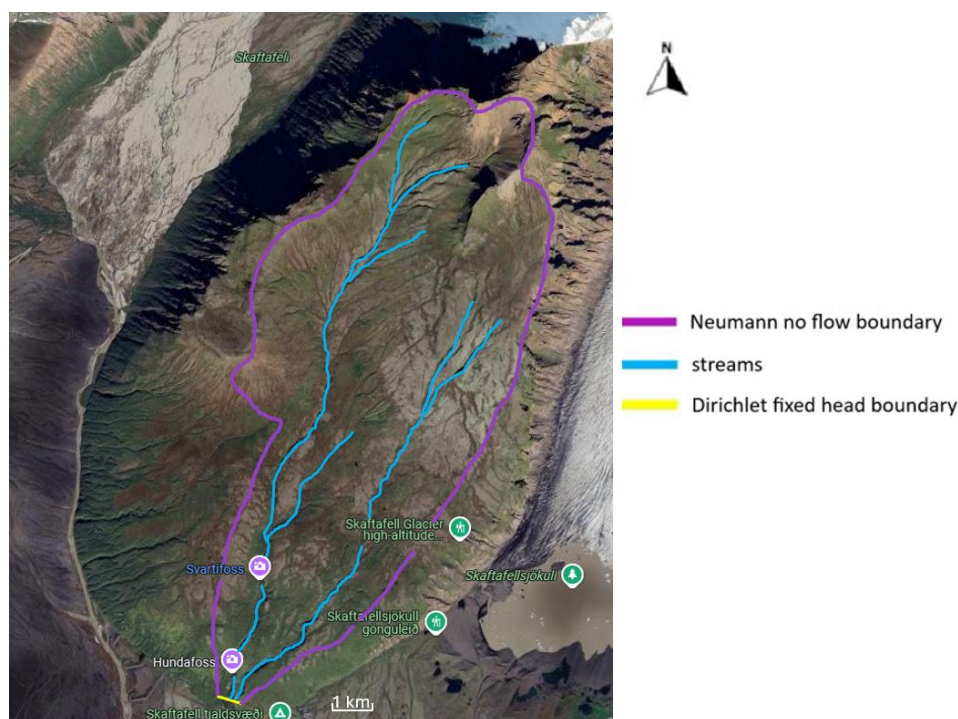

Figure 6. MODFLOW model boundaries and locations of Eystragil (east stream) and Vestragil (west stream).

Reported hydraulic conductivities (k_h and k_v) for fractured and weathered basalts vary between 10^{-4} and 10^2 m d^{-1}, with the highest conductivities found in Hawaiian basalt formations [19]. To narrow down this wide range for this study, fracture density and

fracture width measurements were collected at waterfalls such as Svartifoss, at the flanks of the basalt dome, where the older basalts surface, and at Reynisfjara. For Skaftafellsheiði, it was expected that the REV would be at least 10 times the column diameter, as the spatial uniformity of the basalt columns is mostly unknown. This resulted in an estimated REV of 10m^3 [35]. Due to the structure of columnar basalt jointing, strong anisotropy occurs, with a relatively low k_h and a relatively high k_v within the basalt formation. For the upper layers (basalt 1 and 2), k_h was set to 0.3 m d^{-1} [36]. This k_h is in line with the expectation that, due to the lower horizontal pressure, the fissures are more open than at greater depth. Due to higher pressure on the fractures, and, therefore, a smaller fracture width in the deeper basalt layers, the k_h and k_v of these layers (basalt 3 to 7) were set to 0.01 m d^{-1} [19,37]. At the southern tip of the model, in the top basalt layer (basalt 1), the k_h was increased to 12 m d^{-1}, in line with the values found at Svartifoss. This adjustment helped avoid flooded cells in the model and was justified by the fact that this layer is surfacing at the outlet, thus exerting reduced horizontal pressure on the basalt columns, creating wider voids. On top of the basalt formations, thin layers of peat, regolith, and/or soil were added in accordance with field observations. The k_h and k_v were taken as 5 m d^{-1} for the organic soil layer and peat layer and as 10 m d^{-1} for the regolith layer. Figure 7 provides an overview of the MODFLOW model setup with its topography and model layers. Imaginary drillings were used to force MODFLOW to produce a representative representation of the formations up to the model base at 90 m + msl. Table 3 lists the materials and physical properties of the model layers. The initial model was calibrated with PEST, i.e., a parameter estimation module to obtain optimized sets of parameters. For this optimization, initial values, minimum values, and maximum values were chosen [29]. As can be seen in Figure 7C, the basalt formations decrease in thickness downhill from Skaftafellsheiði. Additionally, a sensitivity analysis was conducted after model calibration. This showed that the k_h of the peat layer and the basalt layer had the greatest influence on the model results.
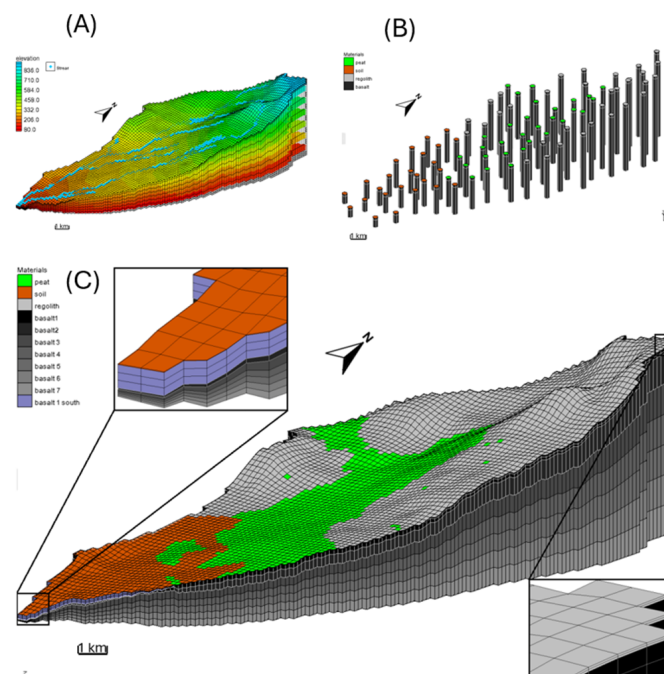
Figure 7. MODFLOW model setup at Skaftafellsheiði, with (**A**) the elevation (m + msl), the layer distribution and the streams, (**B**) the materials added to the imaginary boreholes, and (**C**) the detailed model setup.

**Table 3.** Materials and physical properties of the MODFLOW model layers at Skaftafellsheiði.

| Material	Thickness (m)	k_h (m d^{-1})	k_v (m d^{-1})	Specific Storage (m^{-1})	Specific Yield (−)
organic soil	0.5	5	5	1×10^{-6}	0.08
peat	2–4	5	5	1×10^{-6}	0.2
regolith	2	10	10	1×10^{-6}	0.4
basalt 1	10	0.3	10	1×10^{-6}	0.4
basalt 2	1–134	0.3	0.3	1×10^{-6}	0.4
basalt 3–7	1–134	0.01	0.01	1×10^{-6}	0.4

3. Results

3.1. Field Campaign Results

3.1.1. Precipitation

During the field campaign in 2015 (12 July–6 September 2015), there were only a few small rain showers recorded until mid-August. Then, significant rain was measured for two weeks, before becoming minimal again (Figure 8). The rainfall represents the rainfall at 100 m + msl (rain gauge at the Skaftafell campsite). The largest recorded rain event was 24 mm d^{-1} on 14 August 2015, followed by 22 mm d^{-1} on 15 August 2015.


(**A**)

(**B**)
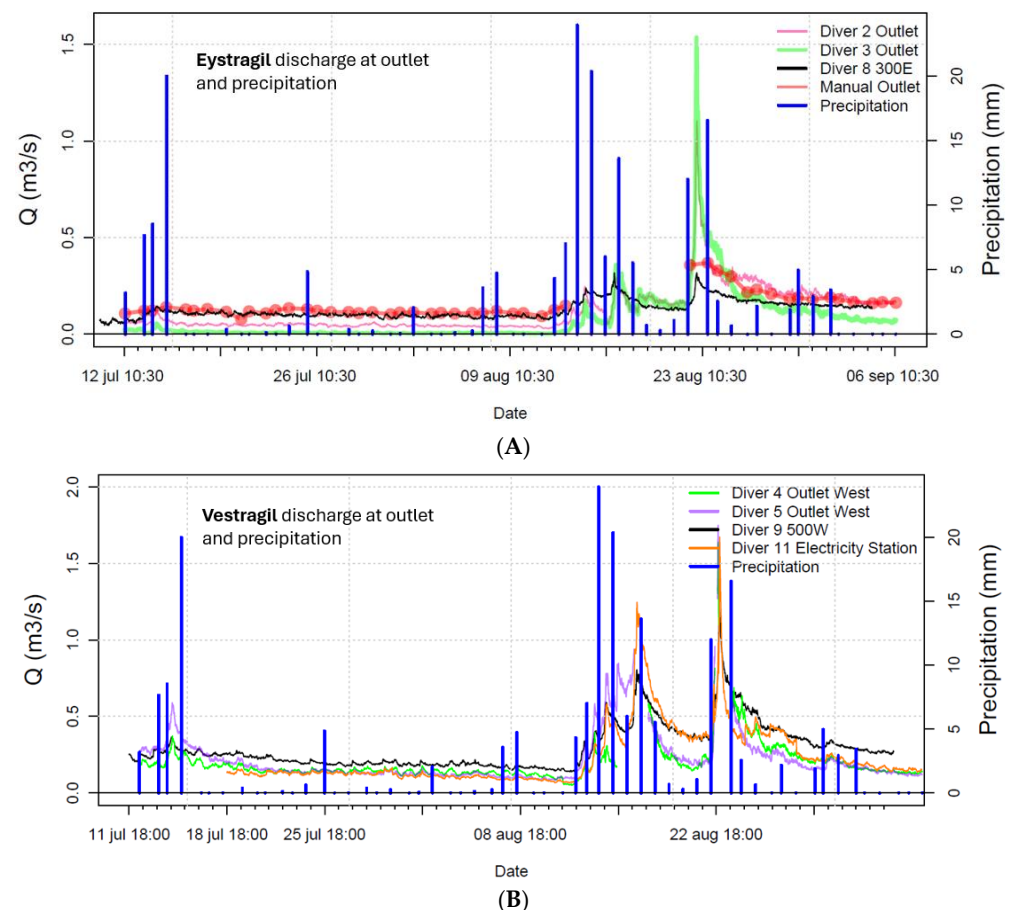
Figure 8. Discharge (Q) and precipitation and discharge of (**A**) Eystragil and (**B**) Vestragil during the 2015 field campaign.

The 2023 campaign began with significant rain, followed by a drier period and then a rain event of >60 mm during the final stages of the campaign (Figure 9).
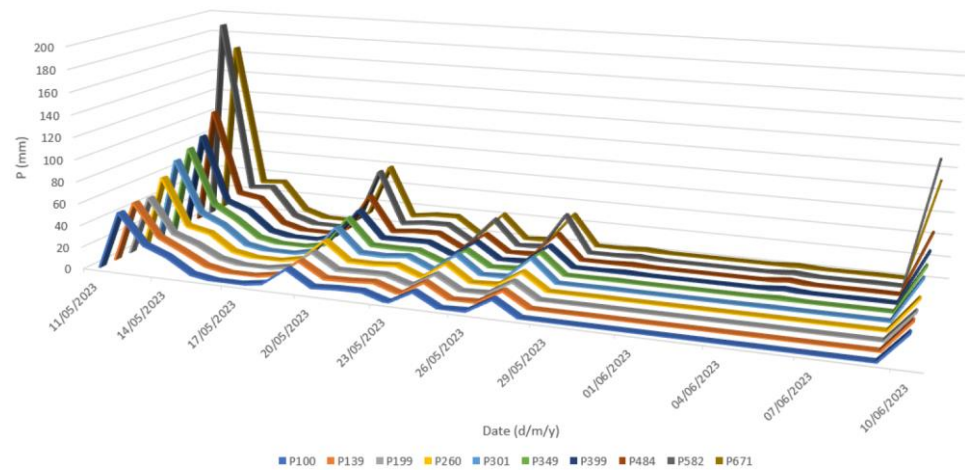
Figure 9. Precipitation along the elevation profile during the 2023 field campaign.

Figure 10 shows the cumulative precipitation per rain gauge at the selected elevations for the period of 11 May–11 June 2023. In the range of 100–200 m + msl, there was no noticeable increase in P with increasing elevation. Upward of 200 m + msl, the precipitation began to increase. At the highest altitudes, the cumulative P was more than twice the P at 110 m + msl. This is in line with the findings of Hannesdóttir et al. [38].
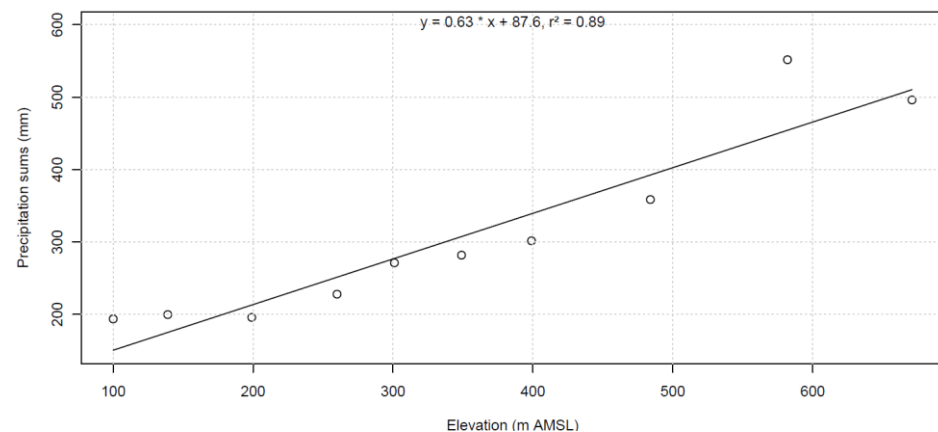
Figure 10. Correlation between elevation and P per rain gauge at Skaftafellsheiði in 2023.

3.1.2. Snowmelt

During the 2015 field campaign (12 July–6 September 2015), snow coverage and snow depth were estimated by calculating the snow-covered area in the higher sections of the catchment and the thickness of the snowpack at multiple locations. It was estimated that, at the start of the field campaign, there was approximately 400×10^3 m^3 of snow in the catchment, an amount that was reduced to approximately 1.5×10^3 m^3 of snow by the end of the same campaign. With a snow–water equivalence of 0.1, an estimated 40×10^3 m^3 and 0.15×10^3 m^3 of water was stored as snow at the start and end of the field campaign, respectively.

During the 2023 field campaign (9 May–11 June 2023), snow was measured several times. At the start of the campaign, the catchment was almost free of snow. During the first few days, some snowfall was observed at higher altitudes, with an average (cumulative) thickness of 5–10 cm on 14 May. With a snow–water equivalence of 0.1, this equals 5–10 mm of water. A few smaller snow events were recorded, with a total snow thickness of 2–4 cm, equal to 2–4 mm of water. At the end of the 2023 campaign, the catchment was free of snow. This implied that no ΔS for snow cover had to be incorporated in the water balance.

3.1.3. Discharge

In 2015, the first part of the short intensive measurement campaign was relatively dry. Discharge hardly responded to rainfall events, indicating sufficient storage capacity. From 12 August 2015 onward, a wet period began. At first, this led to small peaks in discharge and an increase in base flow, but the rainfall event on 22 and 23 August 2015 caused a significant discharge peak, even though the cumulative rainfall was less than that recorded in the period of 12–18 August. Apparently, the storage capacity of the catchment, specifically in the organic soil, peat, and regolith layer, was exceeded at that point. See also Figure 8 for the Eystragil and Vestragil in 2015.

In 2023, the discharge of the Vestragil and Eystragil reacted clearly to the larger P-events on 18 May (20 mm at 100 m + msl), 27 May (15 mm), and 10 June 2023 (35 mm). The Eystragil and Vestragil total discharge was approximately 1×10^6 and 2×10^6 m^3 for the period of 18 May–10 June 2023 (Figure 11). While during the 12 July–6 September 2015 field campaign a clear storage effect was found, no such effect was recorded during the 9 May–11 June 2023 campaign. This can be linked to the difference in timing of the field campaigns, i.e., Icelandic summer in 2015 and Icelandic spring in 2023.
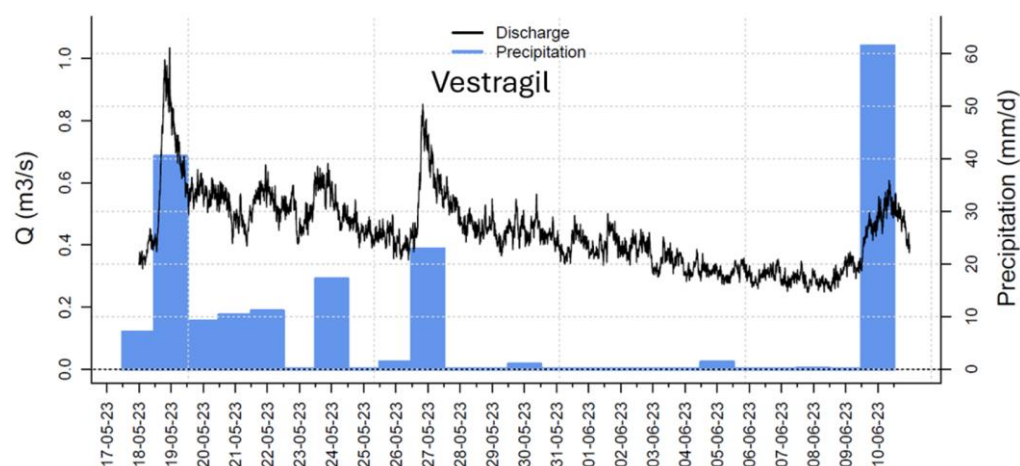

Figure 11. Discharge and daily precipitation in 2023.

3.1.4. Evapotranspiration

Evapotranspiration varies strongly per vegetation zone, and, thus, also across different elevation zones. Figure 12 shows ET_{pot} for the 2015 (Figure 12A) and 2023 (Figure 12B) campaigns, respectively. In 2023, the calculated ET_{pot} for peat (bog), peat (forest), and peat (grass) yielded identical results. Therefore, only peat (grass) is shown in the figure. Different crop factors (K_c) and different land coverages (f_c) resulted in differences in ET_{pot}. In the higher areas with bare regolith, vegetated regolith, and moss coverage, the ET_{pot} was always significantly lower than 2 mm d^{-1}. The lower altitudes with peat and/or deciduous forests had a much larger ET_{pot}. The relative high values are caused by relatively high temperatures in combination with relatively low humidity and long daylight periods. For the 2015 campaign, the total calculated ET_{pot} was 0.66×10^6 m^3, while for the 2023 campaign it was approximately 0.5×10^6 m^3.

ΔET_{pot} averaged for the total field campaign in 2015, all vegetation types, and elevations was 1.4 mm d^{-1}. Averages of ET_{pot} of 3.5 and 2.6 mm d^{-1} were found for July and August 2015, representative of the elevation of 100 m+msl. Einarsson [39,40] reported an ET_{ref} of 3.1 and 2.2 mm d^{-1} for July and August, respectively, at Kirkjubæjarklaustur. This indicates that the calculated values for ET_{ref} and ET_{pot} offer a reasonable estimation for the catchment. Calculated evapotranspiration (1–2 mm d^{-1}) is in line with the literature [1,10]. In the MODFLOW model, best results were obtained when the top layer (organic soil,

peat, and regolith) was considered to be most conductive (up to 10 m d^{-1}), with a gradual reduction in hydraulic conductivity with depth in the basaltic aquifers.
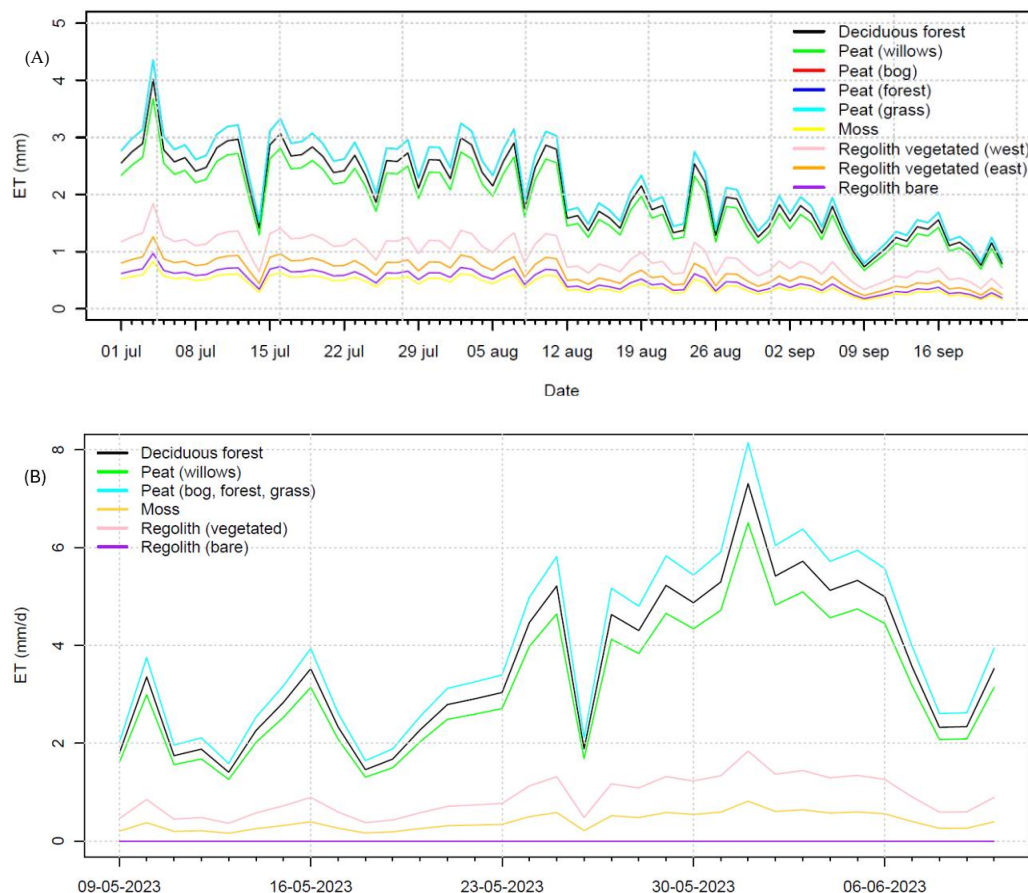
Figure 12. ET_{pot} for each vegetation zone at Skaftafellsheiði for the (**A**) 2015 campaign and (**B**) 2023 campaign.

3.1.5. Water Balance

Table 4 shows the water balance for both field campaigns. Both field campaigns exhibited comparable water balance terms, except for Q in 2023. The 3×10^6 m^3 seems to be an overestimation of the discharge of Vestragil and Eystragil, even though the relative shares of both streams align with the expectations. The ΔS of 2015 supports the conclusion that, despite the rather short field campaign, the measurement was long enough to properly assess the balance components. Summarizing, these values seem to be suitable for use as the upper boundary of a groundwater flow model like MODFLOW.

Table 4. Water balance for the 2015 and 2023 field campaigns.

| Water Balance	*P*	*M*	*Q*	ET_{pot}	ΔS
July/August 2015					
10^6 m^3	2.05	0.24	1.49	0.66	0.14
mm	206	25	150	67	14
May/June 2023					
10^6 m^3	1.9	0.16	3.0	0.50	1.44
mm	190	17	300	51	144

3.2. Modeling Results

The stationary model was fed by a topography-driven recharge rate, in line with the field observations on precipitation and the calculated ET_{pot} (Figure 13A). This resulted in a modeled head distribution, as shown in Figure 13B.
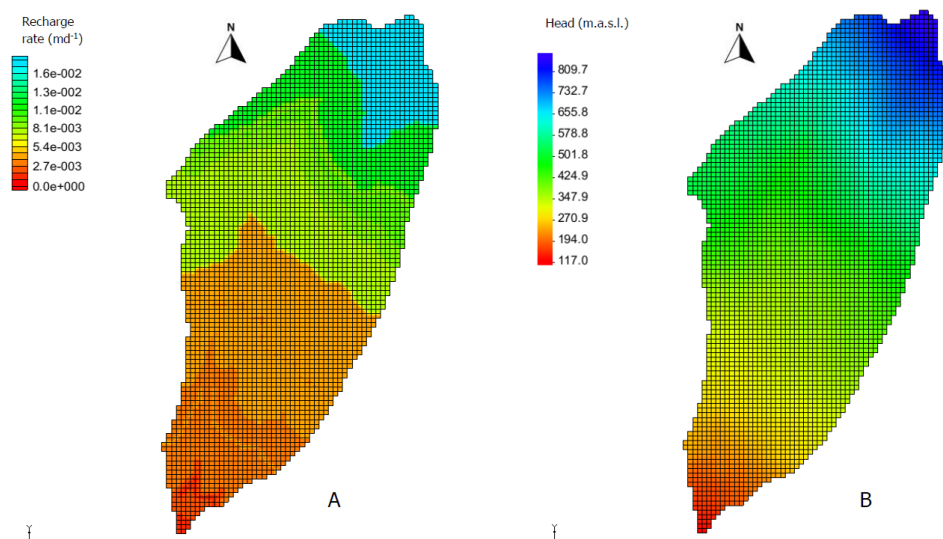
Figure 13. (**A**) Recharge rate (m d^{-1}) and (**B**) calculated head in the stationary model.

As expected, the groundwater follows the topography and drains at the outlet of the Vestragil and Eystragil at 100 m + msl. The addition of the more permeable 'basalt 1 south' prevents the layers in the southernmost part of the model from flooding due to excessively low transmissivity (*kD*). The calculated discharge of Eystragil and Vestragil (approximately 29.5×10^3 m^3 d^{-1}) is comparable to the total measured daily averaged discharge during the July/August 2015 campaign (approximately 31.5×10^3 m^3 d^{-1}). Since no wells in the basaltic aquifers are available [41], the calculated groundwater heads were compared with the locations where shallow water levels were observed during the field campaigns. In the section of 300–500 m + msl, the water heads are slightly overestimated (computed groundwater head up to several meters too high), as shown in Figure 14. This might be caused by the fact that the topography is steeper in the >500 m + msl elevation range than at lower elevations. At the intersect where the topography becomes less steep, the groundwater flow velocity in the basalt fissures slows down, thereby promoting higher groundwater levels. That also happens in the Skaftafellsheiði itself, although the water there is drained by numerous small, shallow streams. These small streams were not incorporated into the model, a fact that implies that the water has to be discharged as groundwater, thus resulting in an excessively high calculated groundwater level. Since the stationary approach was used for the modeling with averaged rain surplus, the model also yielded an average discharge (in m^3 d^{-1}) and no storage change. The modeled stream leakage of both streams did come very close to the measured discharge, i.e., both were in the order of 30×10^3 m^3 d^{-1}. This implies that the field water balance and the model water balance yield similar results.
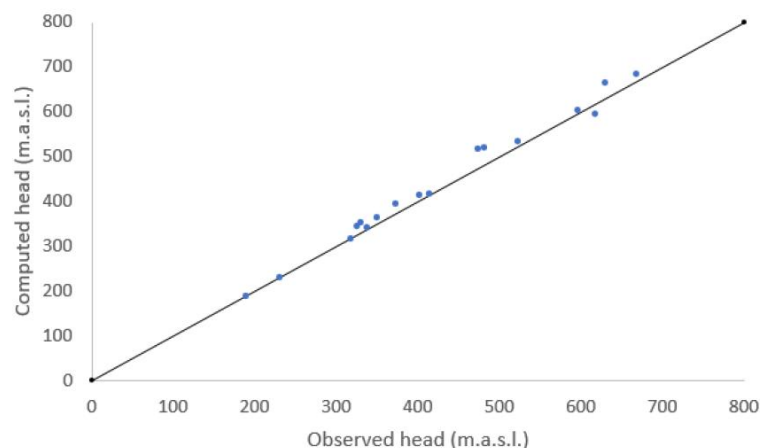
Figure 14. Observed heads during the field campaigns versus the groundwater levels computed with MODFLOW. Dots below the 1/1 line indicate an excessively low computed water head, while dots above the 1/1 line indicate an excessively high computed water head.

4. Discussion

The inaccessibility of basaltic aquifers and the harsh environmental conditions at the Skaftafellsheiði catchment limited the extent of the field campaigns, resulting in a number of uncertainties in the corresponding water balance approach and MODFLOW model results, with such uncertainties discussed here.

Precipitation at Skaftafellsheiði was measured using totalizers, which may be prone to larger errors when, at high altitudes, wind speed impacts the direction of the rain. This may have impacted the total precipitation sum and the findings for the orographic effect. On the other hand, it is expected that the variable wind directions will average out this effect.

During both field campaigns, there was some snow accumulation at higher altitudes in the catchment. However, this snow pack was rather thin (maximum of approximately 10 cm) and short-lived. Therefore, it is assumed that, at least in the instance of these field campaigns, it did not have a significant influence.

During both field campaigns, the discharge was measured at the foot of the basalt dome, where the Vestragil and Eystragil enter the Skeiðararsandur. At this location, a gravel bed of unknown thickness, and thus unknown transmissivity, can absorb part of the discharged water, thereby impacting the accuracy of the discharge measurements. The stage–discharge relationships used for both outlets exhibited a rather good fit, with an R^2 of approximately 0.7. Nevertheless, a setup with a weir would improve the accuracy of the discharge observations significantly.

The calculated ET_{pot} for the 2015 field campaign was 67 mm for the whole measuring period of 56 days, while it was 51 mm for the 2023 campaign of 33 days. This resulted in an ET_{pot} of 1.2 and 1.5 mm d^{-1} for 2015 and 2023, respectively. Einarsson [39,40] found ET_{ref} values in the order of magnitude of 2 to 3 mm d^{-1} for Kirkjubærklaustur. During May/June, the number of daylight hours is 19 hd^{-1}, on average. Based on the rather low number of sunny days during both field campaigns and the use of the crop factor (k_c) and vegetation coverage (f_c) to estimate ET_{pot}, then the calculated ET_{pot} seems to be in line with the literature.

The final water balance calculation showed comparable values (in 10^6 m^3 or in mm for the measuring period) for both field campaigns, even though the period from 12 July to 6 September 2015 had a duration of 56 days and the period from 9 May to 11 June 2023 totaled 33 days. The daily average precipitation in 2023 was almost twice the daily average precipitation in 2015, reaching 6 and 3.7 mm d^{-1}, respectively. The discharge in the 2023

field campaign seems to be overestimated. As a result, the calculated storage change ΔS is also high.

Snowmelt occurring during the summer season is not a large contributing factor in the water balance. In the higher parts of the catchment, some snowfall can occur in spring and early summer. However, this snowpack is mostly rather thin (up to 10 cm), melting away quickly (within days).

The catchment boundaries, constructed by using the topographical boundaries as hydrological boundaries, seem to be rather well chosen. In the case of a significant deep groundwater flow through deeper basalt formations which would not end up at the catchment outlet, then the balance error would be large. The July/August 2015 campaign seems to show that all surface water and groundwater interactions occur in the cover layers and the first few basalt layers.

The model setup was not meant to be an exact representation of the subsequent layers and their physical properties. In other research, it was already found that the spatial variability of the saturated hydraulic conductivity (k_h and k_v)—as measured in field settings—is large [1,3,10]. That was also the case for the field measurements at Skaftafellsheiði. The measurements in the weathered cover (regolith) of the basalt formations yielded values as low as 1 m d^{-1} and as high as >100 m d^{-1}. With a hydraulic conductivity in the range of 2 m d^{-1} for the organic (peat) soils and 9 m d^{-1} for the regolith layer, the top material seems to be well represented in the MODFLOW model. According to the literature, the hydraulic conductivity for fractured and weathered basalt varies between 10^{-4} and 10^2 m d^{-1} [10,18]. The values of 5 m d^{-1} found in this study for k_h and k_v in the upper layers (organic soil and peat), 10 m d^{-1} for regolith, and 0.3 and 10 for k_h and k_v of the basalt in the upper section, reducing with depth to 0.01 m d^{-1}, are well within this range.

Skaftafellsheiði, as an isolated basaltic dome, proved to be an interesting site to combine field experiments and modeling exercises. A limiting factor is that the weather conditions are rather harsh for most of the year, making it difficult to have at least one full hydrological year as a dataset. Automatic weather and ground and surface water level equipment might provide useful data, although it would need regular maintenance. The modeling exercise showed promising results, even though the information on the basalt formations in the deeper subsurface was mostly indirect. Further research might also be conducted in areas with less harsh conditions but with a significant rain surplus and information on deep wells in the basalt formations.

5. Conclusions

Making use of the water balance method through two field campaigns and the frequently used groundwater model MODFLOW, we attempt to better understand the functioning of basaltic aquifers, in particular the one underlying the Skaftafellsheiði catchment.

The output of the modeled water balance in MODFLOW showed that the stream leakage in the model is in the same order as the measured discharge. This indicates that there is a rather good understanding of the catchment's boundaries.

We conclude that the model did offer a rather good representation of groundwater–surface water interactions for the Skaftafellsheiði catchment, even though we did not model all the Tertiary basalt layers in detail. Having a limited number of basalt formations with a reduced k_h, k_v, and porosity with depth was good enough to obtain a good, representative REV to quantify the groundwater and surface water flow. This implies that, when the sampling domain comprises a domain of multiple flows (scale D in Figure 1), then a representative parameter value can be found. At this scale, no detailed information about fracture aperture, degree of connectivity, and smoothness of fractures is required, since they are inside the sample volume. At that point, Darcy's Law can be applied to

describe the water flow, and a groundwater flow model (like MODFLOW) can provide a good representation.

Future research will aim to extend the field campaigns to obtain a year-round overview of P, ET, and discharge dynamics. The model experiments will head toward transient modeling and a more detailed representation of the upper model layers. Hopefully, this will lead to an even better understanding of the interaction between the regolith layer and the underlying basalt aquifers under variable seasonal conditions.

Abbreviations

The following abbreviations are used in this manuscript:

REV　　Representative elementary volume

References

1. Dijksma, R.; Brooks, E.S.; Boll, J. Groundwater recharge in Pleistocene sediments overlying basalt aquifers in the Palouse Basin, USA: Modeling of distributed recharge potential and identification of water pathways. *Hydrogeol. J.* **2011**, *19*, 489–500. [CrossRef]
2. Versey, H.R.; Singh, B.K. Groundwater in Deccan basalts of the Betwa Basin, India. *J. Hydrol.* **1982**, *58*, 279–306. [CrossRef]
3. Candel, J.; Brooks, E.S.; Sanchez-Murillo, R.; Grader, G.; Dijksma, R. Identifying recharge connections in the Moscow (USA) sub-basin using tracers and a soil moisture routing model. *Hydrogeol. J.* **2016**, *24*, 1739–1751. [CrossRef]
4. Brown, K.B.; McIntosh, J.C.; Rademacher, L.K.; Lohse, K.A. Impacts of agricultural irrigation recharge on groundwater quality in a basalt aquifer system (Washington, USA): A multi-tracer approach. *Hydrogeol. J.* **2011**, *19*, 1039–1051. [CrossRef]
5. Taylor, R.G.; Howard, K.W.F. The dynamics of groundwater flow in the regolith of Uganda. *Int. Contrib. Hydrogeol.* **1998**, *18*, 97–114.
6. Gropius, M.; Dahabiyeh, M.; Al Hyari, M.; Brückner, F.; Lindenmaier, F.; Vassolo, S. Estimation of unrecorded groundwater abstractions in Jordan through regional groundwater modelling. *Hydrogeol. J.* **2022**, *30*, 1769–1787. [CrossRef]
7. Hancox, J.; Gárfias, J.; Aravena, R.; Rudolph, D. Assissing the vulnerability of over-exploited volcanic aquifer systems using multi-parameter analysis, Tucola Basin, Mexico. *Environ. Earth Sci.* **2010**, *59*, 1643–1660. [CrossRef]
8. Liu, H.H.; Doughty, C.; Boðvarsson, G.S. An active fracture model for unsaturated flow and transport in fractured rocks. *Water Resour. Res.* **1998**, *34*, 2633–2646. [CrossRef]
9. MacDonald, D.M.J.; Kulkami, H.C.; Lawrence, A.R.; Deolankar, S.B.; Barker, J.A.; Lalwani, A.B. Sustainable groundwater development of hard-rock aquifers: The conflict between irrigation and drinking water supplies from the Deccan basalts of India. In *British Geological Survey NERC Technical Report WC/95/52*; 1995; 54p.
10. Domenico, P.A.; Schwartz, F.W. *Physical and Chemical Hydrogeology*, 2nd ed.; John Wiley and Sons: Hoboken, NJ, USA, 1997; ISBN 978-0-471-59762-9.
11. Dijksma, R.; Avis, L. Measuring and modelling water transport on Skaftafellsheiði, Iceland. *Forum Geogr.* **2016**, *XV*, 66–72. [CrossRef]
12. Pyatt, F.B.; Ditcham, D. A contribution to the study of the ecology of Iceland: The ecology of a scree slope on Skaftafellsheiði and a Sandur area. *Int. J. Environ. Stud.* **1983**, *20*, 299–306. [CrossRef]
13. Grunngerð Landupplýsingátt. Available online: https://kort.gis.is/mapview/ (accessed on 25 February 2025).
14. Guðmundsson, A.T. *Living Earth: Outline of the Geology of Iceland*; Mal og Menning: Reykjavik, Iceland, 2007; ISBN 978-9979-3-3360-9.
15. Helgason, J.; Duncan, R.A. Glacial-interglacial history of the Skaftafell region, southeast Iceland, 0–5 MA. *Geology* **2001**, *29*, 179–182. [CrossRef]

16. Wood, W.W.; Fernandez, L.A.; Back, W.; Rosenshein, J.S.; Seaber, P.R. Volcanic rocks. *Hydrogeology* **1988**, *2*, 353–365.
17. Helgason, J. *Bedrock Geological Map of Skaftafell, SE-Iceland*; Geological Consulting: Reykjavik, Iceland, 2007.
18. Hiscock, K.M.; Bense, V.F. *Hydrogeology: Principles and Practice*; John Wiley and Sons: Hoboken, NJ, USA, 2014.
19. Singal, B.B.S.; Gupta, R.P. *Applied Hydrogeology of Fractured Rocks*; Springer Science and Business Media: Berlin/Heidelberg, Germany, 2010.
20. Wellman, T.P.; Poeter, E.P. Estimating spatially variable representative elementary scales in fractured architecture using hydraulic head observations. *Water Resour. Res.* **2005**, *41*. [CrossRef]
21. Avis, L. Estimating Hydrological Characteristics of a Basaltic Catchment Using Simple Field Measurements and Modelling; a Case Study in Skaftafell National Park, Iceland. Master's Thesis, Wageningen University, Wageningen, The Netherlands, 2016.
22. Beck, H.E.; Zimmermann, N.; McVicar, T.R.; Vergopolan, N.; Berg, A.; Woord, E.F. Present and future Köppen-Geiger climate classification maps at 1-km resolution. *Sci. Data* **2018**, *5*, 180214. [CrossRef]
23. Available online: https://vedur.is/ (accessed on 15 April 2025).
24. Spreen, W.C. A determination of the effect of topography upon precipitation. *EOS Trans. Am. Geophys. Union* **1947**, *28*, 285–290.
25. Winkler, M.; Schellander, H.; Gruber, S. Snow water equivalents exclusively from snow depths and their temporal changes: The Δsnow. *EGU Hydrol. Earth Syst. Sci.* **2021**, *25*, 1165–1187. [CrossRef]
26. Hargreaves, G.H.; Samani, Z.A. Estimating potential evapotranspiration. *J. Irrig. Drain. Div.* **1982**, *108*, 225–230. [CrossRef]
27. Samani, Z. Estimating solar radiation and evapotranspiration using minimum climatological data. *J. Irrig. Drain. Eng.* **2000**, *126*, 265–267. [CrossRef]
28. Valiantzas, J.D. Simplified versions for the Penman evaporation equation using routine weather data. *J. Hydrol.* **2006**, *331*, 690–702. [CrossRef]
29. Zweers, E.A. Hydrological Boundaries of a Basaltic Catchment: In Situ Measurements and Modelling of the Basalt Outcrop in Skaftafellsheiði, Iceland. Master's Thesis, Wageningen University, Wageningen, The Netherlands, 2023.
30. Harbaugh, A.W. MODFLOW-2005, the U.S. Geological Survey modular groundwater model. In *US Geological Survey Techniques and Methods*; 2005; Volume 6-A16.
31. McDonald, M.G.; Harbaugh, A.W. *A Modular Three-Dimensional Finite-Difference Groundwater Flow Model*; US Geological Survey: Reston, VA, USA, 1988.
32. Doherty, J. Calibration and uncertainty analysis for complex environmental models. *Watermark Numer. Comput. Brisb. Aust.* **2015**, 227.
33. Khaleel, R. Scale dependence of continuum models for fractured basalts. *Water Resour. Res.* **1989**, *25*, 1847–1855. [CrossRef]
34. Magnuson, S.O. *Inverse modeling for Field-Scale Hydrologic and Transport Parameters of Fractured Basalt*; Lockheed Idaho Technologies CO: Idaho Falls, ID, USA, 1995; INEL-95/0637.
35. Fetter, C.W.; Kreamer, D. *Applied Hydrogeology*, 5th ed.; Waveland Press Inc.: Long Grove, IL, USA, 2022; ISBN 978-1-4786-4652-5.
36. Kooi, M. Hydrological Responses in a Basaltic Catchment: A Case Study on Iceland. Master's Thesis, Wageningen University, Wageningen, The Netherlands, 2015.
37. Brooks, E.S.; Boll, J.; McDaniel, P.A. A hillslope-scale experiment to measure lateral saturated hydraulic conductivity. *Water Resour. Res.* **2004**, *40*. [CrossRef]
38. Hannesdóttir, H.; Aðalgeirsdóttir, G.; Jóhannesson, T.; Guðmundsson, S.; Crochet, P.; Ágústsson, H.; Pálsson, F.; Magnússon, E.; Sigurðsson, S.Þ.; Björnsson, H. Downscaled precipitation applied in modelling of mass balance and the evolution of souteast Vatnajökull, Iceland. *J. Glaciol.* **2025**, *61*, 799–813. [CrossRef]
39. Einarsson, M.A. Potential evapotranspiration and water balance in Iceland. *Hydrol. Res.* **1972**, *3*, 183–198. [CrossRef]
40. Einarsson, M.A. Climate of Iceland. *Elsevier World Surv. Climatol.* **1984**, *15*, 673–697.
41. Verma, K.; Katpatal, Y. Groundwater monitoring using GRACE and GLDAS data after downscaling within basaltic aquifer system. *Groundwater* **2020**, *58*, 143–151. [CrossRef]